Green Chemistry

Accepted Manuscript

This is an *Accepted Manuscript*, which has been through the Royal Society of Chemistry peer review process and has been accepted for publication.

Accepted Manuscripts are published online shortly after acceptance, before technical editing, formatting and proof reading. Using this free service, authors can make their results available to the community, in citable form, before we publish the edited article. We will replace this *Accepted Manuscript* with the edited and formatted *Advance Article* as soon as it is available.

You can find more information about *Accepted Manuscripts* in the Information for Authors.

Please note that technical editing may introduce minor changes to the text and/or graphics, which may alter content. The journal's standard Terms & Conditions and the Ethical guidelines still apply. In no event shall the Royal Society of Chemistry be held responsible for any errors or omissions in this *Accepted Manuscript* or any consequences arising from the use of any information it contains.

ROYAL SOCIETY OF CHEMISTRY

www.rsc.org/greenchem

Effects of hydrogen and water on the activity and selectivity of acetic acid hydrogenation on ruthenium

Hakan Olcay,[1#] *Ye Xu,*[2†*] *George W. Huber*[3‡*]

[1] Department of Chemical Engineering, University of Massachusetts, Amherst, MA 01003, USA

[2] Center for Nanophase Materials Sciences, Oak Ridge National Laboratory, Oak Ridge, TN 37831, USA

[*] Y. Xu : e-mail: yexu@lsu.edu. G. W. Huber: e-mail: huber@engr.wisc.edu.

[#] Current address: Department of Aeronautics and Astronautics, Massachusetts Institute of Technology, Cambridge, MA 02139, USA.

[†] Current address: Department of Chemical Engineering, Louisiana State University, Baton Rouge, LA 70803, USA.

[‡] Current address: Department of Chemical and Biological Engineering, University of Wisconsin-Madison, Madison, WI 53706, USA.

Green Chemistry Accepted Manuscript

Abstract

Kinetic flow reactor experiments have been carried out to study acetic acid hydrogenation on a Ru/C catalyst in both three-phase (catalyst, aqueous, and gaseous) and two-phase (catalyst and gaseous) regimes. In addition, density functional theory calculations have been carried out to investigate the selective (ethanol formation) and unselective pathways, and the results have been combined with microkinetic modeling to better understand the activity and selectivity observed in the experiments. Our experiments show that ethanol selectivity varies strongly from <10% to a maximum of ~70% with increasing hydrogen partial pressure (p_{H_2}) at 185°C in the three-phase reactor. Co-fed water also enhances ethanol selectivity, from ~60% to ~70% in the two-phase reactor and ~40% to ~65% in the three-phase reactor, at 185°C, but only up to a certain concentration. The aqueous phase is not necessary for high ethanol selectivity. The first-principles microkinetic analysis is able to reasonably capture the apparent activation energy, ethanol selectivity, and reaction orders of acetic acid and ethanol with respect to p_{H_2}, providing a theoretical explanation for the crucial role that hydrogen plays in the selectivity of this reaction. Our findings provide insights into why high activity and selectivity for acetic acid hydrogenation to ethanol can be achieved on Ru, which may have general relevance to the catalytic hydrogenation of organic oxygenates on Ru and other metals.

Green Chemistry Accepted Manuscript

Introduction

Increases in the cost of petroleum combined with growing concerns about the environmental impact of fossil fuels are prompting researchers worldwide to investigate biomass as a feedstock for the production of liquid fuels and commodity chemicals.[1] Biomass feedstock differs from petroleum feedstock in being highly rich in oxygen-containing functional groups. The selective reduction of oxygen in the biomass feedstock will be an integral part of future bio-refineries. Many processes currently being developed for the conversion of biomass into biofuels involve hydrogenation in the aqueous phase. The aqueous phase is an ideal carrier for large hydrophilic molecules and permits mild-temperature processes reducing undesirable decomposition. These processes include the hydrodeoxygenation of bio-oils,[2] hydrogenation of fermentation broths,[3, 4] and alkane production by aqueous phase processing.[5, 6] One of the slowest steps in the hydrotreating of bio-oils is the hydrogenation of organic acids.[7]

Ru/C has been shown to be an excellent aqueous-phase hydrogenation (APH) catalyst for organic acids. Miller and co-workers converted lactic[3, 8, 9] and propionic[3] acids to the corresponding aldehydes and alcohols on Ru/C catalysts by APH at 70-150°C and 30-100 bar of hydrogen pressure (p_{H_2}). They reported high activity and selectivity (up to 95%) toward propylene glycol from lactic acid.[8] We have shown that Ru/C has the highest activity and ethanol selectivity in the APH of acetic acid among several monometallic transition metal catalysts (Ru, Rh, Pt, Pd, Ir, Ni, and Cu) at mild temperature and up to ~50 bar of p_{H_2}.[4] Supported Ru catalysts can also hydrogenate many other organic oxygenates with high activity and selectivity.[10-14] All this stands in contrast to the reactivity of Pt group metals at UHV and low-pressure conditions, which

Green Chemistry Accepted Manuscript

leads primarily to C-C bond scission in acetic acid,[15-21] although alloying[18] and strong interaction with oxides[19, 22, 23] can markedly alter the selectivity in favor of ethanol. These studies show that the main challenge with conversion of oxygenates over Ru catalysts is selectivity, and that the reaction conditions play a crucial role.

Previously, we have demonstrated that the high activity of a Ru/C catalyst relative to other metals at given conditions can be explained by the ability of Ru to activate the initial C-O bond scission.[4] The origin of the high ethanol selectivity, which stands in contrast to the UHV and ambient pressure experiments, remains unclear and unaddressed in the existing literature. We have, therefore, carried out a series of kinetic experiments to explore what is responsible for the selectivity for ethanol in the hydrogenation of acetic acid on Ru/C. Selectivity to ethanol (Equation 1) is entirely a kinetic phenomenon since CH_4 and CO_2 are the thermodynamically more favored products via decarbonylation (Equation 2) and decarboxylation (Equation 3):

$$CH_3COOH_{(g)} + 2H_{2(g)} \rightarrow CH_3CH_2OH_{(g)} + H_2O_{(g)} \quad \Delta G^{\circ}_{rxn}=\text{-}13.6 \text{ kJ/mol} \qquad (1)$$

$$CH_3COOH_{(g)} + H_{2(g)} \rightarrow CH_{4\,(g)} + CO_{(g)} + H_2O_{(g)} \quad \Delta G^{\circ}_{rxn}=\text{-}33.4 \text{ kJ/mol} \qquad (2)$$

$$CH_3COOH_{(g)} \rightarrow CH_{4\,(g)} + CO_{2(g)} \quad \Delta G^{\circ}_{rxn}=\text{-}62.0 \text{ kJ/mol} \qquad (3)$$

Our experiments indicate that higher p_{H_2} strongly favors ethanol formation vs. non-selective C-C bond cleavage of acetic acid. Furthermore, co-feeding water is found to promote the ethanol selectivity in both the three-phase and two-phase regimes, whereas the three-phase conditions are not necessary to obtain high ethanol selectivity. The strong effects of p_{H_2} are further corroborated by density functional theory (DFT) calculations and microkinetic analysis based on a mechanism involving the dissociation

Green Chemistry Accepted Manuscript

of acetic acid and the hydrogenation of the monoxy (C_xH_yO) intermediates. The effects of H_2 and water on acetic acid conversion and ethanol formation have been noted in previous batch reactor experiments,[24, 25] but to our knowledge detailed kinetic experiments and first-principles-based theoretical analysis have not been performed before for acetic acid hydrogenation on Ru.

In the following, we first recap the results of a set of experiments previously carried out in the three-phase flow reactor varying the temperature as the main variable, but here we provide more detailed analysis of the reaction conditions, as a change in temperature entailing a corresponding change in other variables such as p_{H_2}. We then describe the results of our new experiments, in which the partial pressures/concentrations of H_2 and water have been varied while holding other variables constant, in order to demonstrate the effects of H_2 and water on the activity and selectivity of this reaction on Ru/C. In the remaining portion of this article we present a DFT study of the reaction pathways and the results of microkinetic analysis, which demonstrates that our theoretical understanding can explain both the activity and ethanol selectivity of this reaction on Ru.

Methods

Experimental

All experiments are carried out in a continuous up-flow packed-bed reactor over a 5% Ru/C catalyst (Evonik H1, Strem Chemicals). The catalyst, obtained as 50% wetted, is first dried overnight at 100°C unless indicated otherwise. It is then reduced *in situ* under a hydrogen flow of 155 mL/min at 290°C for two hours following an 8-hour temperature ramping. Based on the electrochemical behavior of Ru[26, 27] and previous experiments

Green Chemistry Accepted Manuscript

employing Ru in aqueous solutions,[10, 28] we conclude that the Ru catalysts in our study are stable against oxidation or dissolution in the O_2-free acetic acid solution with an initial concentration of 10 wt% (or 3.2 mol%; pH=2.3) under high p_{H_2}.[4] The metal dispersion of the fresh catalyst is measured, via hydrogen adsorption with Quantachrome Autosorb 1C, to be 6.7%.

Acetic acid (glacial, Fisher) feed (with or without water) is pumped by an HPLC pump (Jasco PU980) into the reactor system. The aqueous feed then mixes with hydrogen (and helium as an inert gas, when dilution is needed), and enters a ¼" OD tubular stainless steel reactor. The reactor runs through a cylindrical aluminum insert that is used to provide better heat conduction and is placed inside a tubular split furnace (Lindberg) that is heated to the desired reaction temperature. The liquid feed is heated up or evaporated, depending on the reaction conditions, on glass beads packed within the reactor between two end-plugs of glass wool (Fisher). Reaction takes place over the catalyst packing fixed between the two sets of glass wool. After the reaction, the effluent cools down at the exit of the reactor. Another set of glass beads is used after the catalyst packing to prevent the condensed phase at the exit of the reactor from coming in contact with the reacting phase(s) on the catalyst surface. The cooled-down products separate into different phases in a 150 mL sample cylinder (Swagelok). The gaseous products are analyzed on-line. The liquid products are drained from the phase separator periodically and analyzed off-line. A back-pressure regulator (Swagelok) is used to keep the reactor pressure constant at desired values.

Three gas chromatographs are employed in the analyses: Hydrogen and carbon dioxide are separated in Hayesep DB packed column and detected using thermal

Green Chemistry Accepted Manuscript

conductivity detector (HP 5890II GC). Gaseous and liquid hydrocarbons are separated in AT-Q capillary column and analyzed by flame ionization detector (HP 5890II GC). Liquid products are also analyzed by a Shimadzu GC-2010 Plus system equipped with FID and Restek RTX-VMS capillary column.

The reaction parameters for the experiments performed in this study are described in various tables. The set values indicate the parameters physically set on the experimental setup at *normal temperature and pressure* (NTP), i.e. 20°C and 1 atm. The volumetric flow rates of the *gas-phase* acetic acid-water mixture (for the two-phase reactions), and of hydrogen and helium at the *reaction temperature and pressure* (RTP) are calculated in the following way: The compressibility factors (Z) calculated using the Peng-Robinson equation of state[29] are used in the non-ideal gas law, $pV=ZnRT$, to calculate the molar densities (V/n) of hydrogen and helium at NTP, which are used to obtain the inlet molar flow rates ($\dot{n}$) using the volumetric flow rates ($\dot{V}$) at NTP. From the inlet molar flow rates, the volumetric flow rates at RTP can then be obtained. The volumetric and molar flow rates of the *liquid-phase* acetic acid-water mixture (for the three-phase reactions) at the reaction temperature are calculated through the density equations given by Sun et al.[30] Whether the acetic acid-water mixture remains in the liquid phase or is vaporized at the reaction temperature and pressure is determined through dew point and bubble point calculations. If the calculated bubble point pressure is below the total pressure then the mixture is assumed to remain in the liquid phase. If the calculated dew point pressure is above the total pressure then the mixture is assumed to completely evaporate into gas phase. The concentration for a species A is calculated

Green Chemistry Accepted Manuscript

by taking the ratio of the inlet molar flow rate of A ($\dot{n}_A$) to the sum of individual volumetric flow rates of all species ($\dot{V}_i$) in all phases (ϕ) at RTP:

$$c_A = \sum_{\phi} \frac{\dot{n}_A}{\sum_i \dot{V}_i} \quad (4)$$

The total pressure, along with the other parameters to be set at NTP on the experimental system, is varied in a trial-and-error procedure controlled by a computer program to achieve the concentrations at the reaction conditions that are to be tested. The liquid hourly space velocities and gas hourly space velocities (LHSV and GHSV, respectively) are calculated from the volumetric flow rates at RTP and the volume of the catalyst packing unless indicated otherwise.

Theoretical

Spin-polarized periodic DFT calculations are performed in the generalized gradient approximation (GGA-PBE)[31] using the Vienna Ab initio Simulation Package (VASP).[32] The core electrons are described by the PAW method,[33] and the Kohn-Sham valence states are expanded in a plane wave basis set up to a kinetic energy of 400 eV. A first-order Methfessel-Paxton scheme is used for the smearing of electronic states with a smearing factor of 0.075. All total energies are extrapolated to 0 K.

The equilibrium bulk lattice constants for Ru are calculated to be 2.726/1.578 Å, in good agreement with the experimental values of 2.70/1.58 Å.[34] The surfaces of bulk Ru are represented by the thermodynamically most stable (0001) surface, which is in line with the low dispersion of our Ru/C catalyst. Ru step edges are expected to be poisoned by low molecular weight carbon-containing species from decomposition at moderate temperatures.[4, 35, 36] The (0001) surface is modeled by a (3×3) surface unit cell consisting

Green Chemistry Accepted Manuscript

four layers of metal atoms and is separated from neighboring slabs in the z direction by seven layers equivalent of vacuum. The surface Brillouin zone is sampled with a 5×5×1 Monkhorst-Pack k-point mesh. The total energy of the slab changes by 0.05 eV of sampling by a 7×7×1 Monkhorst-Pack k-point mesh, and the energy per layer of the four-layer slab differs by 0.01 eV from that of a five-layer slab. Thus, we consider the energies to be converged with respect to the given parameters.

Adsorption is allowed on one side of the slab only, with dipole decoupling.[37] All adsorbates and the top two Ru layers are relaxed, and the bottom two Ru layers are held fixed at bulk positions. Geometry optimization is converged to below 0.03 eV/Å in each degree of freedom for all relaxed atoms. The binding energy (ΔE) of an adsorbate is calculated as $\Delta E = E_{\text{total}} - E_{\text{clean}} - E_{\text{gas}}$, where E_{total}, E_{clean}, and E_{gas} are the total energies of the slab with the adsorbate on it, the clean metal slab without any adsorbate, and the adsorbate atomic, radical, or molecular species in the neutral state in the gas phase, respectively. The (3×3) surface unit cell corresponds to a coverage (θ) of 1/9 ML for one adsorbate per unit cell.

The free energy of a gas-phase species, A, is calculated as:[38]

$$G_{\text{A}} = E_{\text{A}} + E_{\text{A}}^{ZPE} + \Delta h_{\text{A}}\left(T, p^0\right) - Ts_{\text{A}}\left(T, p^0\right) + k_B T \ln\left(\frac{p_{\text{A}}}{p^0}\right) \qquad (5)$$

The pressure dependence of G_{A} enters through p_{A}, with the reference pressure p^0 being 1 bar. Δh_{A} is $h(T, p^0) - h(0\text{ K}, p^0)$ and the values of the enthalpies and entropies of the gas-phase species tabulated by NIST were used.[39] E_{A} and E_{A}^{ZPE} are the DFT total energy and zero-point energy (ZPE) of A in gas phase. k_{B} is the Boltzmann constant. The gas-phase conformation used in this study for acetic acid is the more stable *cis*-(C=O, C-OH).

Green Chemistry Accepted Manuscript

For an adsorbed species A*, its free energy is calculated as:[40]

$$G_{A^*} = E_{A^*} + E_{A^*}^{ZPE} + \Delta u_{A^*}(T) - Ts_{A^*}(T) \quad (6)$$

where Δu_{A^*} replaces Δh for gas-phase species and is the change in internal energy from 0 K to T. E_{A^*} is the DFT total energy of the species A when adsorbed on the surface and is equal to $E_{total} - E_A$, with E_{total} being the total energy of the surface plus the adsorbate. E^{ZPE}, Δu_{A^*}, and s_{A^*} are calculated from the vibrational frequencies associated with the normal modes of the gas-phase or adsorbed species. The normal modes are calculated in the harmonic approximation by diagonalizing the mass-weighted Hessian matrix, which was built from calculated two-sided differences of the first derivatives of the total energy due to small geometrical perturbations (0.01 Å) in each degree of freedom of the optimized geometry of A*.

The minimum-energy reaction path and transition state (TS) for each elementary step is determined using a combination of the climbing-image nudged elastic band method[41, 42] and the dimer method[43] as appropriate. Each TS is verified to possess only one imaginary mode in the direction of the corresponding bond breaking/forming process. The free energy of the TS complex is calculated as described above for an adsorbed species, except with the imaginary mode excluded.

Results and Discussion

Effects of temperature

Previously, we reported the effect of temperature on the activity and selectivity of the APH of acetic acid over a 5% Ru/C catalyst, the results of which are summarized here.[4] The experiments were carried out at a constant total pressure of 750 psi and three

Green Chemistry Accepted Manuscript

different temperatures (110, 160, and 185°C). The reaction parameters are given in Table 1. At 750 psi and below 246°C, the content of the reactor remains as a three-phase mixture (gas phase, aqueous phase, and catalyst). We follow previous examples and assume our reactor to behave as a differential reactor because the conversion was less than 20%.[44, 45] Our previous work also included experiments at 245°C,[4] but those results are excluded here because the conversion was greater than 20%. The apparent activation energy (E_a^{app}),

$$E_a^{app} = -k_B \left(\frac{\partial(\ln(r))}{\partial(1/T)} \right)_{p_i} \quad (7)$$

for acetic acid conversion was calculated to be 33 kJ/mol (or 0.35 eV; Figure 1), somewhat lower than the 53.1 kJ/mol reported by Shih et al. for the hydrogenation of acetic acid on Ru in a batch reactor.[24] The ethanol selectivity was 84% at 110°C and 74% at 185°C. The main side products included ethyl acetate, acetaldehyde, and alkanes (mainly methane), while CO and CO_2 were detected only at ppm levels.

Effects of hydrogen pressure

Increasing temperature causes $p_{H_2O}^{sat}$ to increase and concurrently p_{H_2} to decrease at a fixed total pressure. Thus, the temperature experiments (Tables 1-2) actually varied temperature and p_{H_2} together. To isolate the effect of p_{H_2}, we have performed two additional sets of experiments, both with the concentration of acetic acid held constant and the hydrogen concentration allowed to vary. Here hydrogen concentration is taken to be directly proportional to p_{H_2} at constant T because of the ideal gas behavior and low solubility in water of hydrogen. In the first set shown in Table 3, the hydrogen

Green Chemistry Accepted Manuscript

concentration was varied at a fixed reactor temperature of 160°C by allowing the total pressure to increase from 250 to 750 psi. Both the rate of acetic acid conversion and the ethanol selectivity increased with increasing total pressure (Figure 3). Since the water partial pressure was constant at constant temperature, the change in total pressure was entirely due to an increase in the inlet p_{H_2}. Experiments by Shih et al. carried out in three-phase conditions using a batch reactor led to similar conclusions on a Ru catalyst.[24]

Another way to change p_{H_2} was to add an inert gas (helium) to the gas stream while maintaining a constant total gas flow rate as shown in Table 4. The temperature, total pressure, and inlet liquid concentrations were also held constant. The total molar flow rate, the volumetric flow rate of acetic acid plus water, and the concentration of acetic acid were identical to those used at 185°C in Table 1 when no helium was added. Figure 4 shows the effect of changing the hydrogen concentration on the turnover frequency (TOF) and product selectivity. The ethanol selectivity increased and the ethane and methane selectivity decreased (Figure 4a), while the overall TOF of acetic acid increased slightly, with increasing hydrogen concentration (Figure 4b). As expected, *adding* an inert gas such as He at constant temperature and pressure had the same effect as *lowering* the partial pressure of H_2 by decreasing the overall pressure. At 185ºC, diluting H_2 significantly reduced the selectivity for ethanol while promoting undesired C-C and 2nd C-O dissociation products, primarily methane and ethane. CO and CO_2 were detected only at ppm levels over the range of H_2 concentration tested and are therefore ignored.

Green Chemistry Accepted Manuscript

If the reaction rates can be written as a power law with respect to H_2 concentration, then on a log-log scale the slope of the TOF versus H_2 concentration gives the apparent reaction orders with respect to p_{H_2} (a_{H_2}); i.e.,

$$a_{p_{H_2}} = \left(\frac{\partial\left(\ln\left(r\right)\right)}{\partial\left(\ln\left(p_{H_2}\right)\right)} \right)_T \quad (8)$$

The TOF of acetic acid conversion and ethanol, methane, and ethane formation are plotted as a function of H_2 concentration on a log-log scale in Figure 4b. The TOF of methane and ethane formation clearly deviate from straight lines, indicating that the rate equations for the two species cannot be expressed as a simple power law. The TOF of acetic acid also deviates from a straight line, but less so than the TOF of methane and ethane. Fitting a straight line to the rate of acetic acid conversion yields an apparent reaction order with respect to hydrogen concentration of 0.20. A reaction order of 0.4-0.6 with respect to p_{H_2} was reported previously for acetic acid hydrogenation on Pt/TiO_2.[19] The TOF for ethanol formation is much closer to being linear, and its apparent reaction order with respect to hydrogen concentration is 1.38.

Effects of water concentration

Besides hydrogen concentration, another factor affecting the ethanol selectivity is the water concentration. Figure 5 shows the effect of water concentration based on the sum of the liquid-phase (if any) and gas-phase flow rates on the TOF and selectivity for acetic acid and the major products. The concentration of acetic acid and the ratio of the acetic acid:H_2 concentrations were both kept constant in these experiments (see Table 5 for experimental parameters). The temperature was fixed at 185°C, while the total pressure

Green Chemistry Accepted Manuscript

was varied so that the reaction takes place in the two-phase regime as well as the three-phase regime for comparison. These experiments were carried out at lower hydrogen concentrations compared to the preceding experiments to accentuate the effect of water.

For the rates of ethanol, methane and ethane formation, the calculated apparent reaction orders are 0.74, 0.51 and 0.33, respectively, in the two-phase regime, and 0.60, -0.26 and 0.17, respectively, in the three-phase regime. In the two-phase regime, increasing the concentration of co-fed water mildly enhanced the ethanol selectivity by ca. 10% (mainly at the expense of methane; Figure 5a) and consistently increased the TOF of acetic acid conversion (Figure 5b). On the other hand, in the three-phase regime an over 20% increase in the ethanol selectivity was obtained by increasing the concentration of co-fed water, while the rate of acetic acid conversion remained nearly constant. In both the two-phase and the three-phase regimes, increasing water concentration was beneficial to ethanol selectivity up to a certain point, beyond which it had little additional effect (Figure 5a). The highest rate of acetic acid conversion and the highest ethanol selectivity were obtained in the two-phase regime. At the given conditions, the TOF of acetic acid conversion was somewhat lower in the three-phase regime than in the two-phase regime. However, aqueous phase reactions may be beneficial from an economic point of view, because the process excludes an expensive step such as volatilization.

The exact mechanism for the beneficial effects of water is unclear. Since water is a product of the reaction, one might expect increased concentration of water in the reactant stream to decrease the rate of the reaction according to Le Châtelier's principle if the system is in equilibrium. As the microkinetic models suggest (see following

Green Chemistry Accepted Manuscript

sections), the reaction is far from equilibrium under given conditions, so water does not affect the reaction thermodynamically. Possible explanations for the enhancement effect of water include: 1) Water stabilizes the desired product, ethanol. Although acetic acid and ethanol both have appreciable vapor pressures under standard conditions and although the reaction does not have to be carried out in aqueous phase unlike larger organic molecules, the high affinity of ethanol for water may help stabilize ethanol relative to CO_2 and alkanes, which are the thermodynamically more stable products than ethanol in gas phase as mentioned in the Introduction. 2) Water enhances bond scission/formation steps through hydrogen bonding or proton shuttling.[46] However, to the extent that the formation of both ethanol and decomposition products involve C-H bond scission/formation, and that the stabilizing effect of water on the less polar C-H bond is not as significant as on the C-O bond,[47] the significance of the kinetic effect of water on the selectivity of this reaction is unclear. 3) Water dissociation on Ru provides a source of oxidant to remove surface poisons, e.g. removing CO through water-gas shift that would produce additional hydrogen *in situ*. This could explain why water benefits both the activity and selectivity of this reaction. However, the production of CO and CO_2 was at the ppm levels, whereas methane was consistently the main side product, indicating that residual carbon is primarily removed reductively, not oxidatively. Overall, the beneficial role of water in acetic acid hydrogenation requires further study to be fully understood.

Reaction mechanism for ethanol formation

In a previous study,[4] we concluded that the rate of acetic acid conversion on different metal catalysts can be understood as controlled by the rate of the first C-O bond scission

Green Chemistry Accepted Manuscript

step for acetic acid, and that the first C-O bond scission occurs directly in acetic acid or acetate on Ru(0001). Here we investigate the reaction pathway from acetic acid to ethanol on Ru(0001) in more detail. Following C-O bond scission in acetic acid or acetate, the successive hydrogenation of acetyl (CH_3CO) may give rise to a series of monoxy intermediates, including acetaldehyde (CH_3CHO), 1-hydroxyethylidene (CH_3COH), 1-hydroxyethyl (CH_3CHOH), ethoxy (CH_3CH_2O), comprising three different pathways to ethanol. Figure 6 shows the snapshots of the minimum-energy configurations of these intermediates (see Table 6 for the corresponding adsorption energies). Figure 6 also shows the reaction network for the formation of ethanol from acetic acid hydrogenation based on these intermediates, along with the activation and reaction energies of the elementary steps in the network. All bond scission/formation steps are assumed to be surface-mediated, as has been done in previous works on aqueous-phase catalytic conversion of organic acids.[3, 4, 19, 48]

In Table 7, the TS energies of the various monoxy hydrogenation steps are listed. It can be seen that the acetyl→acetaldehyde→ethoxy pathway has the lowest overall activation energy. We designate this the primary hydrogenation pathway (see Figure 7 for snapshots of the TS's on this pathway). Esterification forming ethyl acetate is not included here for simplicity because a variety of processes, including metal-free, acid-catalyzed ones, may produce esters from acetic acid.[23, 49]

Descriptor for ethanol selectivity

The non-selective decomposition of acetic acid to alkanes may be initiated anywhere along the selective pathway. For this reason, we have investigated how the monoxy surface intermediates, including acetyl, acetaldehyde, 1-hydroxyethylidene, and 1-

Green Chemistry Accepted Manuscript

hydroxethyl, decompose via C-C, 2nd C-O, and methyl C-H bond scission, which we designate as the primary decomposition steps. The decomposition of further dehydrogenated species ($CH_{x<3}R$) is not investigated because previous studies have shown that they tend to undergo facile C-C bond scission.[18, 50] C-C bond scission in acetic acid and acetate is not considered further because of the significant activation energies for these steps (DFT total energy E_a=1.33 and 1.70 eV, respectively).

We propose that the ethanol selectivity can be estimated by comparing the rate of the primary decomposition step with the *lowest*-energy TS, to that of the primary hydrogenation step with the *highest*-energy TS. A comparison of the primary decomposition steps shows that the TS of methyl C-H scission in acetaldehyde (acetaldehyde→ketenal) is the lowest in energy, whereas ethoxy→ethanol is the primary hydrogenation step with the highest-energy TS (Table 7). By assuming that the steps leading up to acetaldehyde and ethoxy formation are quasi-equilibrated compared to methyl C-H scission in acetaldehyde and ethoxy hydrogenation to ethanol, respectively, the rates of the decomposition and hydrogenation of monoxy intermediates are seen as controlled by the following two *lumped* steps:[50]

$$CH_3COOH_{(g)} + {}^1/_2\, H_{2(g)} + 3* \leftrightarrow (CH_2CHO)^{*}\cdots H^{*\ddagger} + OH^{*} \quad (9)$$

$$CH_3COOH_{(g)} + {}^3/_2\, H_{2(g)} + 2* \leftrightarrow (CH_3CH_2OH)^{*\ddagger} + OH^{*} \quad (10)$$

The rates of these two steps are given by the transition state theory as:

$$r_{decomp} = \frac{k_B T}{h} \cdot e^{-\frac{G^{\neq\circ}_{decomp} + G^{\circ}_{OH} - G^{\circ}_{AA} - \frac{1}{2}G^{\circ}_{H_2}}{k_B T}} \cdot \frac{p_{AA}\, p_{H_2}^{\frac{1}{2}}\, \theta_*^3}{\theta_{OH}} \quad (11)$$

Green Chemistry Accepted Manuscript

$$r_{hydrog} = \frac{k_B T}{h} \cdot e^{-\frac{G^{\ddagger\circ}_{hydrog} + G^{\circ}_{OH} - G^{\circ}_{AA} - \frac{3}{2}G^{\circ}_{H_2}}{k_B T}} \cdot \frac{p_{AA} p_{H_2}^{\frac{3}{2}} \theta_*^2}{\theta_{OH}} \quad (12)$$

here h is the Planck constant. The ratio of the two rates is:

$$S = r_{hydrog} / r_{decomp} = e^{-\frac{G^{\ddagger\circ}_{hydrog} - G^{\ddagger\circ}_{decomp} - G^{\circ}_{H_2}}{k_B T}} \cdot \frac{p_{H_2}}{\theta_*} \quad (13)$$

and the ethanol selectivity is therefore $S/(S+1)$. The standard free energies for the two TS's (TS_{hydrog} and TS_{decomp}) are listed in Table 8.

S and θ_* are solved for together iteratively through the microkinetic models as described below. As formulated, the selectivity descriptor, S, is a function of gas-phase H_2 through both the p_{H_2} and the $G^{\circ}_{H_2}$ terms. This is consistent with the experimental insights, and we shall see below that it also leads to satisfactory theoretical predictions for ethanol selectivity based on DFT calculations.

Microkinetic models of acetic acid hydrogenation to ethanol

The purpose of our microkinetic models is not to simulate a chemical reactor but to predict the TOF and selectivity based on the proposed reaction mechanism and given reaction conditions, using the thermodynamic and kinetic parameters that are entirely derived from DFT calculations (except for the enthalpies and entropies of the gas-phase species, for which tabulated values are used; see Methods). The predictions are to be compared with the observed activity and selectivity, thus providing a measure of the validity of the proposed reaction mechanism.

Green Chemistry Accepted Manuscript

In the present work we propose a simplified reaction mechanism consisting of the following nine of the steps shown in Figure 6 that include the primary hydrogenation pathway, i.e.,

I. $\text{acetic acid}_{(g)} + 2^* \leftrightarrow \text{acetyl}^* + \text{OH}^*$
II. $\text{acetyl}^* + \text{H}^* \leftrightarrow \text{acetaldehyde}^* + *$
III. $\text{acetaldehyde}^* + \text{H}^* \leftrightarrow \text{ethoxy}^* + *$
IV. $\text{ethoxy}^* + \text{H}^* \leftrightarrow \text{ethanol}_{(g)} + 2^*$
V. $\text{O}^* + \text{H}^* \leftrightarrow \text{OH}^* + *$
VI. $\text{OH}^* + \text{H}^* \leftrightarrow \text{H}_2\text{O}_{(g)} + 2^*$
VII. $\text{H}_{2(g)} + 2^* \leftrightarrow 2\text{H}^*$
VIII. $\text{acetic acid}_{(g)} + 2^* \leftrightarrow \text{acetate}^* + \text{H}^*$
IX. $\text{acetate}^* + * \leftrightarrow \text{acetyl}^* + \text{O}^*$

For simplicity, the weakly adsorbing species, including acetic acid, water, and ethanol (cf. Table 6), are ignored so that these species react from/form into the gas phase directly. For acetate, the η^2 configuration has been seen in our calculations at high coverage, in which both of the carboxylic O atoms coordinate to a single Ru atom.

The microkinetic model is solved self-consistently for the coverages of the surface intermediates and the ethanol selectivity as described above, for each of the three sets of conditions used in the temperature experiments (Table 1), by assuming all surface species to be at steady state, i.e., $\frac{d\theta_i}{dt} = 0$, and by including the selectivity descriptor as described above, which simplifies the microkinetic model by neglecting the large numbers of non-selective steps.

As will be shown below, the coverages of all surface species are lower than 0.01 ML under the experimental conditions except for acetate, O, and H. Given the negligible interactions between the monoxy species ($C_xH_yO_z$) suggested by the low coverages, and

Green Chemistry Accepted Manuscript

given the unknown nature of how free sites, hydrogen, and water are arranged around the organic species to affect the adsorption and reaction of the organic species, we use the DFT results at 1/9 ML without co-adsorbed species to calculate the standard free energies for the monoxy species and the TS's, and parameterize them with respect to temperature ($G°(T)$; Table 8). The forward standard activation free energy (G_a°) for a step i is calculated as the difference between the $G°$ of the TS and the sum of the $G°$ of the reactants:

$$G_{a,i}^\circ = G_{TS,i}^\circ - \sum G_{\text{reactants},i}^\circ \tag{14}$$

The forward and backward reaction rate constants for the step are then calculated as:

$$k_{f,i} = \frac{k_B T}{h} e^{-\frac{G_{a,i}^\circ}{k_B T}}, \text{ and } k_{r,i} = \frac{k_{f,i}}{K_i} \tag{15}$$

where K_i is the equilibrium constant for step i. Possible co-adsorbate interactions, e.g. between the organic species, water, O/OH, and hydrogen, and the determination of the interaction energetics will be the subject of future studies. For acetate, atomic O, and atomic H, which are the more abundant surface species, we express their differential standard free energies as functions of both coverage and temperature (Table 8).

The effective partial pressures of the gas-phase species, including acetic acid, hydrogen, water, and ethanol, are determined based on the experimental conditions of the temperature experiments (Table 1) and the predicted selectivity. In our experiments the content of the reactor can either be three-phase or two-phase. In the three-phase regime, the gas phase contains water vapor taken to be at its saturation pressure ($p_{\text{H}_2\text{O}} = p_{\text{H}_2\text{O}}^{sat}(T)$); hydrogen; and small amounts of acetic acid and ethanol (with decomposition products

Green Chemistry Accepted Manuscript

ignored). The partial pressures of acetic acid and ethanol (p_{AA} and p_{EtOH}) are calculated as the saturation pressure corresponding to the average concentration between the inlet and outlet of each species (zero at inlet for ethanol) in the aqueous phase according to Henry's Law (for acetic acid: k_H° = 5400 mol/(kg·bar); $d(\ln(k_H/d(1/T)))$ = 6300 K; for ethanol: k_H° = 190 mol/(kg·bar); $d(\ln(k_H/d(1/T)))$ = 6600 K[39]). Since the solubility of H_2 in water is very low (0.00078 mol/(kg·bar); $d(\ln(k_H/d(1/T)))$ = 500 K[39]), H_2 remains predominantly in the gas phase and the balance of the total pressure is assigned to p_{H_2} (in the absence of helium). Since the decomposition products are ignored in this procedure, p_{H_2} is slightly overestimated particularly at low ethanol selectivity. The calculated effective partial pressures are listed in Table 9.

The predicted TOF of acetic acid conversion ($-r_1$, the net rate of Step I, which is equal to the rate of ethanol formation, the net rate of Step IV, by the steady-state assumption), the coverage for each surface species (θ), and the reversibility (β) of each step predicted by the model are listed in Table 9. The low surface coverage of O species corroborates that the metallic Ru surface is not oxidized under the reaction conditions. The first set of results are based on acetic acid and acetate each dissociating over a pair of sites (the two-site model). The predicted TOF and ethanol selectivity are plotted in Figures 1 and 2 for comparison with the experimental TOF and selectivity. The predicted TOF is too low by two orders of magnitude at 110°C but comes within a factor of ~5 from the measured TOF at 185°C. The ethanol selectivity decreases continuously with the increase in temperature, but the decrease is too rapid compared to the experiments. The E_a^{app} is measured experimentally to be 0.33 eV, whereas the E_a^{app} based on the

Green Chemistry Accepted Manuscript

calculated TOF is 0.78 eV. Incidentally, the alternate acetyl→1-hydroxyethylidene→1-hydroxyethyl→ethanol and acetyl→acetaldehyde→1-hydroxyethyl→ethanol pathways lead to TOF that are ~10 times smaller (results not shown). These alternate pathways are therefore omitted from subsequent analysis.

The vanishing coverage of free sites coupled with the two-site requirement for C-O bond dissociation appears to be the primary reason for the under-prediction of the TOF at the lower temperatures. To address this inconsistency between the experimental and predicted TOF, we have also tested an *ad hoc* one-site ansatz. It involves changing the free site requirement for the C-O dissociation steps from 2 to 1, i.e.,

I. acetic $acid_{(g)} + * \leftrightarrow acetyl^* + OH^*$

IX. $acetate^* \leftrightarrow acetyl^* + O^*$

and re-solving the model with all other parameters kept the same. The results of this modified model (the one-site model) are also listed in Table 9 and plotted in Figures 1 and 2 for comparison. The TOF of the one-site model agrees more closely with the experiments, and the selectivity is overall in better agreement with the experiments (Figure 2). The predicted E_a^{app} is now 0.59 eV, also in closer agreement with the experiments than the two-site model is. Whereas in the two-site model the acetic acid channel is the dominant C-O bond scission mechanism ($\beta_1 >> \beta_9$), the acetate channel is somewhat more dominant ($\beta_9 > \beta_1$) in the one-site model.

The one-site ansatz may be rationalized in the following way: The scission of the carboxylate C-O bond requires a triangular ensemble of three metal atoms on close-packed metal surfaces (see Figure 7).[51, 52] This precludes the adsorption of other species in the threefold site in the center of the ensemble, and so the TS effectively occupies one

Green Chemistry Accepted Manuscript

threefold site just like H, O, and OH. It should be noted that, whereas most of the organic species bond to Ru(0001) through C or O to the top of Ru atoms, the atomic species as well as OH and ethoxy occupy the threefold sites, so a single site-type in any Langmuir-Hinshelwood reaction mechanism to represent the hydrogenation of acetic acid or other organic oxygenates may be inherently deficient. Two different site-types may need to be invoked,[3] together with an improved description of how intermediates are co-adsorbed on the surface, in order to more accurately describe this reaction with microkinetic or kinetic Monte Carlo modeling. Interestingly, the two-site and one-site TOF values bracket the experimental measurements, with the former better matching the experimental values at the higher temperatures and the latter better matching the experimental values at the lower temperatures. Whether this is a reflection of an actual transition from a one-site to a two-site C-O bond scission mechanism remains to be determined.

Both the two-site and the one-site models predict a highly covered surface at all three of the temperatures, with the free site coverage being on the order of ~10^{-4}, and atomic H being the most abundant surface species followed by up to 20% of O and 30% of acetate. According to both models, all the other surface species have negligibly small coverages (omitted from Table 9). Including direct interactions between major surface species may lead to a significantly higher coverage of free sites.[53] It remains to be seen what effect a significant increase in free site coverage would have on the ethanol selectivity. The reaction quotient indicates that the overall reaction is far from equilibrium to the side of the reactants in both models.

Both models predict the ethanol selectivity to decrease with increasing temperature in agreement with the experiments, which suggests that the ethanol

Green Chemistry Accepted Manuscript

selectivity is affected by p_{H_2}. To further probe the effects of hydrogen on the reaction, we have calculated the TOF of acetic acid conversion and ethanol formation at several different values of p_{H_2} (including 5, 10, and 20 bar and the p_{H_2} corresponding to 185°C in the temperature experiment), assuming the same temperature and acetic acid conversion as for the 185°C temperature experiment. The results show that the TOF of both acetic acid conversion and ethanol formation indeed increases with increasing p_{H_2} (Figure 4c). The two-site model predicts the apparent reaction orders with respect to p_{H_2} (a_{H_2}) to be 0.003 for acetic acid conversion and 1.09 for ethanol formation. The one-site model predicts a_{H_2} to be 0.30 and 1.29, respectively, in better agreement with a_{H_2} exhibited in the experiments (0.20 and 1.38, respectively; cf. Figure 4b). The predicted positive a_{H_2} for ethanol formation demonstrates that high p_{H_2} is a requisite for high ethanol selectivity. Furthermore, the positive a_{H_2} are consistent with the calculated reversibility that suggests the hydrogenation steps to be rate-controlling, and corroborates the validity of the selectivity descriptor R. The descriptor does not account for the distribution of different decomposition products, including CH_4, C_2H_6, and CO_2 (see Table 2). More detailed microkinetic analysis will be needed to fully account for the formation of the different decomposition products.

Conclusions

We have performed a series of kinetic flow reactor experiments to better understand the high selectivity for ethanol that can be achieved in acetic acid hydrogenation on Ru. The reaction has a measured E_a^{app} of 33 kJ/mol for acetic acid conversion and well over 70%

Green Chemistry Accepted Manuscript

selectivity for ethanol at and below 185°C in the three-phase (gaseous, aqueous, and catalyst) regime at a fixed total pressure of 750 psi. Microkinetic models based on the dissociative adsorption of acetic acid and the successive hydrogenation of acetyl to acetaldehyde and ethoxy, using DFT-calculated thermodynamic and kinetic parameters except for the enthalpies and entropies of the gas-phase species, are able to predict the rate of acetic acid conversion to within an order of magnitude of the experimental rates, with an calculated E_a^{app} of 0.78 eV (0.59 eV) depending on whether C-O bond scission is taken to occur over two sites or one site.

Our experiments clearly show that increasing the hydrogen pressure increases both the ethanol selectivity and the rate of ethanol formation. This conclusion is closely corroborated by including a simple theoretical selectivity descriptor in the microkinetic model that is based on the rates of the most difficult of the hydrogenation steps and the most facile of the decomposition steps, for the monoxy intermediates ($C_xH_yO_z$). The predicted ethanol selectivity is 72% (two-site model) and 85% (one-site model) at 110°C and decreases with increasing temperature, in close agreement with the experimental results (84% at 110°C). Moreover, at 185°C and a total pressure of 750 psi (three-phase regime), the measured TOF of acetic acid conversion and ethanol formation have an apparent reaction orders of 0.20 and 1.38 in hydrogen concentration, respectively, with which the predicted apparent reaction orders also come in good agreement (0.003 and 1.09 (two-site model), and 0.30 and 1.29 (one-site model)). Co-feeding water is identified as another way to enhance the ethanol selectivity in both the three-phase and two-phase regimes, up to a certain concentration. We offer some thoughts on the origin of the water effect, but its exact mechanism remains to be clarified. Our findings provide

Green Chemistry Accepted Manuscript

insights into why high activity and selectivity for acetic acid hydrogenation can be achieved on Ru, which may have general relevance and applicability for the hydrogenation of organic oxygenates on Ru and other metals, for both two- and three-phase thermal catalytic hydrogenation reactions.

Acknowledgments

Experimental work was performed at University of Massachusetts and supported with a grant from the ACS Petroleum Research Fund. Theoretical work was performed at the Center for Nanophase Materials Sciences, which is sponsored at Oak Ridge National Laboratory (ORNL) by the Scientific User Facilities Division, Office of Basic Energy Sciences, U.S. Department of Energy (US-DOE), and used computing resources of ORNL and the National Energy Research Scientific Computing Center, which is supported by Office of Science, US-DOE, under Contract DE-AC02-05CH11231. G. W. Huber was supported as part of the Institute for Atom-efficient Chemical Transformations (IACT), an Energy Frontier Research Center funded by the US-DOE, Office of Science, Office of Basic Energy Sciences.

Green Chemistry Accepted Manuscript

References

1. G. W. Huber, S. Iborra and A. Corma, *Chem. Rev.*, 2006, **106**, 4044-4098.
2. T. P. Vispute, H. Zhang, A. Sanna, R. Xiao and G. W. Huber, *Science*, 2010, **330**, 1222-1227.
3. Y. Q. Chen, D. J. Miller and J. E. Jackson, *Ind. Eng. Chem. Res.*, 2007, **46**, 3334-3340.
4. H. Olcay, L. Xu, Y. Xu and G. W. Huber, *ChemCatChem*, 2010, **2**, 1420–1424.
5. G. W. Huber, R. D. Cortright and J. A. Dumesic, *Angew. Chem. Int. Ed.*, 2004, **43**, 1549-1551.
6. R. Xing, A. V. Subrahmanyam, H. Olcay, W. Qi, G. P. van Walsum, H. Pendse and G. W. Huber, *Greem Chemistry*, 2010, **12**, 1933-1946.
7. D. C. Elliott, *Energ. Fuels*, 2007, **21**, 1792-1815.
8. Z. G. Zhang, J. E. Jackson and D. J. Miller, *Ind. Eng. Chem. Res.*, 2002, **41**, 691-696.
9. T. S. Dalavoy, J. E. Jackson, G. M. Swain, D. J. Miller, J. Li and J. Lipkowski, *J. Catal.*, 2007, **246**, 15-28.
10. P. Gallezot, N. Nicolaus, G. Fleche, P. Fuertes and A. Perrard, *J. Catal.*, 1998, **180**, 51-55.
11. E. P. Maris and R. J. Davis, *J. Catal.*, 2007, **249**, 328-337.
12. K. P. Pimparkar, D. J. Miller and J. E. Jackson, *Ind. Eng. Chem. Res.*, 2008, **47**, 7648-7653.
13. L. E. Manzer, *App. Catal. A-Gen.*, 2004, **272**, 249-256.

Green Chemistry Accepted Manuscript

14. J. Lee, Y. Xu and G. W. Huber, *Appl. Catal. B-Environ.*, 2013, **140–141**, 98-107.

15. C. J. Houtman, N. F. Brown and M. A. Barteau, *J. Catal.*, 1994, **145**, 37-53.

16. A. R. Garcia, J. L. da Silva and L. M. Ilharco, *Surf. Sci.*, 1998, **415**, 183-193.

17. R. D. Haley, M. S. Tikhov and R. M. Lambert, *Catal. Lett.*, 2001, **76**, 125-130.

18. R. Alcalá, J. W. Shabaker, G. W. Huber, M. A. Sanchez-Castillo and J. A. Dumesic, *J. Phys. Chem. B*, 2005, **109**, 2074-2085.

19. W. Rachmady and M. A. Vannice, *J. Catal.*, 2000, **192**, 322-334.

20. G. Hoogers, D. C. Papageorgopoulos, Q. Ge and D. A. King, *Surf. Sci.*, 1995, **340**, 23-35.

21. M. Bowker, C. Morgan and J. Couves, *Surf. Sci.*, 2004, **555**, 145-156.

22. R. Pestman, R. M. Koster, J. A. Z. Pieterse and V. Ponec, *J. Catal.*, 1997, **168**, 255-264.

23. G. Onyestyák, *Catal. Commun.*, 2013, **38**, 50-53.

24. Y. S. Shih and C. K. Lee, *J. Chin. Chem. Soc. (Taipei)*, 1985, **32**, 29-34.

25. H. Wan, R. V. Chaudhari and B. Subramaniam, *Energ. Fuels*, 2012, **27**, 487-493.

26. *CRC Handbook of Chemistry and Physics*, CRC Press, Boca Raton, FL, 2009.

27. T. Loucka, *J. Appl. Electrochem.*, 1989, **20**, 522-523.

28. W. C. Ketchie, E. P. Maris and R. J. Davis, *Chem. Mater.*, 2007, **19**, 3406-3411.

29. S. I. Sandler, *Chemical and Engineering Thermodynamics*, Wiley, 1999.

30. T. Sun, D. Ly and A. S. Teja, *Ind. Eng. Chem. Res.*, 1995, **34**, 1327-1331.

31. J. J. Perdew, K. Burke and M. Ernzerhof, *Phys. Rev. Lett.*, 1996, **77**, 3865.

32. G. Kresse and J. Furthmüller, *Phys. Rev. B*, 1996, **54**, 11169.

33. G. Kresse and D. Joubert, *Phys. Rev. B*, 1999, **59**, 1758.

Green Chemistry Accepted Manuscript

34. N. W. Ashcroft and N. D. Mermin, *Solid State Physics*, Saunders College, Orlando, FL, 1976.

35. P. Ferrin, D. Simonetti, S. Kandoi, E. Kunkes, J. A. Dumesic, J. K. Nørskov and M. Mavrikakis, *J. Am. Chem. Soc.*, 2009, **131**, 5809–5815.

36. S. B. Vendelbo, M. Johansson, D. J. Mowbray, M. P. Andersson, F. Abild-Pedersen, J. H. Nielsen, J. K. Nørskov and I. Chorkendorff, *Top. Catal.*, 2010, **53**, 357-364.

37. J. Neugebauer and M. Scheffler, *Phys. Rev. B*, 1992, **46**, 16967.

38. M. V. Bollinger, K. W. Jacobsen and J. K. Nørskov, *Phys. Rev. B*, 2003, **67**, 085410.

39. R. Sander, in *NIST Chemistry WebBook, NIST Standard Reference Database Number 69*, eds. P. J. Linstrom and W. G. Mallard, National Institute of Standards and Technology, Gaithersburg MD, 2012.

40. M. P. Andersson, E. Abild-Pedersen, I. N. Remediakis, T. Bligaard, G. Jones, J. Engbwk, O. Lytken, S. Horch, J. H. Nielsen, J. Sehested, J. R. Rostrup-Nielsen, J. K. Nørskov and I. Chorkendorff, *J. Catal.*, 2008, **255**, 6-19.

41. G. Henkelman and H. Jónsson, *J. Chem. Phys.*, 2000, **113**, 9978.

42. G. Henkelman, B. P. Uberuaga and H. Jónsson, *J. Chem. Phys.*, 2000, **113**, 9901.

43. G. Henkelman and H. Jónsson, *J. Chem. Phys.*, 1999, **111**, 7010-7022.

44. A. D. Cowan, R. Dumpelmann and N. W. Cant, *J. Catal.*, 1995, **151**, 356-363.

45. M. J. Vincent and R. D. Gonzalez, *App. Catal. A-Gen.*, 2001, **217**, 143-156.

46. C. D. Taylor and M. Neurock, *Curr. Opin. Solid St. M.*, 2005, **9**, 49-65.

Green Chemistry Accepted Manuscript

47. X. Nie, M. R. Esopi, M. J. Janik and A. Asthagiri, *Angew. Chem. Int. Ed.*, 2013, **52**, 2459-2462.

48. B. N. Zope, D. D. Hibbitts, M. Neurock and R. J. Davis, *Science*, 2010, **330**, 74-78.

49. Y. Liu, E. Lotero and J. G. Goodwin Jr, *J. Catal.*, 2006, **242**, 278-286.

50. R. Alcalá, M. Mavrikakis and J. A. Dumesic, *J. Catal.*, 2003, **218**, 178-190.

51. V. Pallassana and M. Neurock, *J. Catal.*, 2002, **209**, 289-305.

52. L. Xu and Y. Xu, *Catal. Today*, 2011, **165**, 96-105.

53. J. Lu, S. Behtash, M. Faheem and A. Heyden, *J. Catal.*, 2013, **305**, 56-66.

Green Chemistry Accepted Manuscript

Tables

Table 1: Parameters in the temperature experiments on acetic acid (AA) hydrogenation.

T (°C)		110	160	185
Set values				
% Liquid concentration	AA		10.00	
Volumetric flow rate (cc/min)	Liquid		0.100	
	H_2		155	
	He		0	
LHSV (1/h)			4.1	
Calculated values				
Molar flow rate (mol/min)	Total		0.0117	
	AA		1.69×10^{-4}	
	H_2O		5.07×10^{-3}	
	H_2		6.46×10^{-3}	
	He		0	
Volumetric flow rate (cc/min)	AA-H_2O	0.106	0.111	0.114
	H_2	4.03	4.55	4.81
	He	0	0	0
Concentration (mol/L)	AA	0.0407	0.0361	0.0342
	H_2O	1.22	1.08	1.03
	H_2	1.56	1.38	1.31
	He	0	0	0
	H_2/AA	38.3	38.3	38.3

Total pressure is 750 psi. Catalyst is Ru/C (0.85 g, 5%). Reaction is in 3-phase regime. Set values are parameters physically set at 20°C and 1 atm. LHSV is weight-based. Calculated values are inlet values based on the reaction temperature and pressure. Concentration is based on the molar and volumetric flow rates.

Green Chemistry Accepted Manuscript

Table 2: Measured activity and selectivity for acetic acid hydrogenation in the temperature experiments.

T (°C)	110	160	185
Carbon conversion (%)	2.936	12.269	16.611
Carbon TOF (1/h)	20.823	86.862	120.702
% Carbon selectivity			
acetaldehyde	0.970	0.185	0.128
ethanol	83.663	80.207	73.952
ethyl acetate	12.638	11.254	10.322
methane	1.867	7.137	13.971
ethane	0.863	1.218	1.627
propane	0	0	0
CO	0	0	0
CO_2	0	0	0

Green Chemistry Accepted Manuscript

Table 3: Parameters in the hydrogen pressure experiments on acetic acid (AA) hydrogenation.

P (psi)		250	500	750
Set values				
% Liquid concentration	AA		10.00	
Volumetric flow rate (cc/min)	Liquid		0.100	
	H_2		155	
	He		0	
LHSV (1/h)			6.0	
Calculated values				
Molar flow rate (mol/min)	Total		0.0117	
	AA		1.68×10^{-4}	
	H_2O		5.05×10^{-3}	
	H_2		6.44×10^{-3}	
	He		0	
Volumetric flow rate (cc/min)	AA-H_2O		0.111	
	H_2	13.5	6.79	4.55
	He	0	0	0
Concentration (mol/L)	AA	0.0124	0.0244	0.0361
	H_2O	0.370	0.731	1.08
	H_2	0.473	0.933	1.38
	He	0	0	0
	H_2/AA	38.3	38.3	38.3

Temperature is 160°C. Catalyst is Ru/C (1.0 g, 5%). Reaction is three-phase. Set values are parameters physically set at 20°C and 1 atm. LHSV is weight-based. Calculated values are inlet values based on the reaction temperature and pressure. Concentration is based on the molar and volumetric flow rates at RTP.

Green Chemistry Accepted Manuscript

Table 4: Parameters in the H_2 concentration experiments on acetic acid (AA) hydrogenation.

Set values					
% Liquid concentration	AA	10.00	9.90	10.00	10.00
Volumetric flow rate	Liquid	0.100	0.099	0.095	0.100
(cc/min)	H_2	155	102	50	20
	He	0	52	98	136
Calculated values					
Molar flow rate	Total	0.0117	0.0116	0.0111	0.0117
(mol/min)	AA	1.69×10^{-4}	1.65×10^{-4}	1.60×10^{-4}	1.68×10^{-4}
	H_2O	5.07×10^{-3}	5.02×10^{-3}	4.79×10^{-3}	5.05×10^{-3}
	H_2	6.46×10^{-3}	4.25×10^{-3}	2.08×10^{-3}	8.31×10^{-4}
	He	0	2.17×10^{-3}	4.07×10^{-3}	5.65×10^{-3}
Volumetric flow rate	AA-H_2O	0.114	0.112	0.108	0.114
(cc/min)	H_2	4.81	3.17	1.55	0.621
	He	0	1.60	3.02	4.19
Space velocity (1/h)	LHSV	4.96	4.87	4.70	4.96
	GHSV	209.	207.	199.	209.
Concentration (mol/L)	AA	0.0342	0.0338	0.0342	0.0342
	H_2O	1.03	1.03	1.02	1.03
	H_2	1.31	0.868	0.444	0.169
	He	0	0.443	0.870	1.15
	H_2/AA	38.3	25.7	13.0	4.94

Temperature is 185°C, and total pressure is 750 psi. Catalyst is Ru/C (0.50 g, 5%). Reaction is three-phase. Set values are parameters physically set at 20°C and 1 atm. LHSV is weight-based. Calculated values are inlet values based on the reaction temperature and pressure. Concentration is based on the molar and volumetric flow rates.

Green Chemistry Accepted Manuscript

Table 5: Parameters in the water concentration experiments on acetic acid (AA) hydrogenation.

P (psi)		100	120	140	220	240	260
Set values							
Liquid concentration (%)	AA	28.54	15.40	10.40	28.54	15.44	10.46
Volumetric flow rate (cc/min)	Liquid	0.028	0.050	0.074	0.014	0.024	0.037
	H_2	126.4	120.1	120.3	63.2	57.8	60.1
	He	0	0	0	108	113	132.1
Calculated values							
Reaction		2-phase	2-phase	2-phase	3-phase	3-phase	3-phase
Molar flow rate (mol/min)	Total	6.54×10^{-3}	7.51×10^{-3}	8.85×10^{-3}	7.76×10^{-3}	8.31×10^{-3}	9.91×10^{-3}
	AA	1.37×10^{-4}	1.31×10^{-4}	1.30×10^{-4}	6.86×10^{-5}	6.27×10^{-5}	6.52×10^{-5}
	H_2O	1.14×10^{-3}	2.39×10^{-3}	3.72×10^{-3}	5.72×10^{-4}	1.15×10^{-3}	1.86×10^{-3}
	H_2	5.25×10^{-3}	4.99×10^{-3}	5.00×10^{-3}	2.63×10^{-3}	2.40×10^{-3}	2.50×10^{-3}
	He	0	0	0	4.49×10^{-3}	4.70×10^{-3}	5.49×10^{-3}
Volumetric flow rate (cc/min)	AA-H_2O	6.79	11.1	14.4	0.0160	0.0273	0.0420
	H_2	29.1	23.0	19.8	6.62	5.55	5.33
	He	0	0	0	11.3	10.8	11.7
Space velocity (1/h)	LHSV	0	0	0	2.83	4.83	7.43
	GHSV	6352	6035	6053	3172	2894	3014
Concentration (mol/L)	AA	3.82×10^{-3}	3.82×10^{-3}	3.79×10^{-3}	3.82×10^{-3}	3.82×10^{-3}	3.82×10^{-3}
	H_2O	0.0319	0.0700	0.109	0.0319	0.0698	0.109
	H_2	0.146	0.146	0.146	0.146	0.146	0.146
	He	0	0	0	0.250	0.286	0.322
	H_2:AA	38.3	38.3	38.6	38.3	38.3	38.3

Temperature is 185°C. Catalyst is Ru/C (0.12 g, 5%, dry). Set values are parameters physically set at 20°C and 1 atm. Calculated values are inlet values based on the reaction temperature and pressure. The liquid space velocity under normal conditions was kept within the ranges of 2.48-6.55/h and 4.96-13.1/h for three-phase and two-phase reactions, respectively. Concentration is based on the molar and volumetric flow rates.

Green Chemistry Accepted Manuscript

Table 6: Minimum-energy adsorption configuration and energies (ΔE, in eV) of surface intermediates on Ru(0001).

	configuration	ΔE	ΔZPE
acetic acid	μ-O,H	-0.49	-0.02
acetate	μ-O,O	-3.13	+0.08
acetyl	C off top	-2.41	+0.08
acetaldehyde	C off top	-0.72	+0.04
1-hydroxyethylidene	C off top	-2.74	+0.04
ethoxy	O hcp	-2.74	+0.16
1-hydroxyethyl	C atop	-1.69	+0.08
ethanol	O atop	-0.40	+0.03
O	hcp	-5.90	+0.08
OH	O fcc	-3.32	+0.12
H_2O	flat, atop	-0.40	+0.07
H	fcc	-2.87	+0.16

All energies are in eV. ΔE is based on DFT total energies. Adding ΔZPE (in eV) to ΔE yields ZPE-corrected adsorption energy. Coverage is 1/9 ML.

Green Chemistry Accepted Manuscript

Table 7: Free (G°_{TS}, in eV) and total (E°_{TS}, in eV) energies of the transition states of the primary hydrogenation and decomposition steps for the monoxy intermediates.

Step		T (°C) 110	160	185	
			G°_{TS}		E°_{TS}
acetyl+H → acetaldehyde		0.41	0.45	0.47	0.50
acetaldehyde+H → ethoxy		0.61	0.67	0.70	0.42
ethoxy+H → ethanol		0.71	0.79	0.83	0.31
acetyl+H → 1-hydroxyethylidene		0.68	0.70	0.71	0.98
acetaldehyde+H → 1-hydroxyethyl		1.00	1.07	1.10	0.89
1-hydroxyethylidene+H → 1-hydroxyethyl		1.02	1.08	1.11	0.54
1-hydroxyethyl+H → ethanol		0.65	0.75	0.80	0.32
acetyl:	C-C	0.73	0.73	0.72	1.26
	C-O	0.74	0.74	0.75	1.20
	C-H	0.67	0.67	0.67	1.24
acetaldehyde:	C-C	1.28	1.32	1.34	1.39
	C-O	1.12	1.16	1.17	1.22
	C-H	0.31	0.34	0.36	0.49
1-hydroxyethylidene:	C-C	1.12	1.12	1.12	1.39
	C-O	0.71	0.74	0.76	0.83
	C-H	0.61	0.65	0.66	0.76
1-hydroxyethyl:	C-C	1.62	1.68	1.71	1.44
	C-O	1.00	1.06	1.08	0.81
	C-H	0.81	0.88	0.91	0.61
ethoxy:	C-C	2.04	2.10	2.12	1.92
	C-O	1.00	1.06	1.09	0.80
	C-H	0.75	0.82	0.85	0.54

All energies are in eV. All TS's are calculated at 1/9 ML coverage. Free energies are calculated at the conditions of the temperature experiments (Table 1). E°_{TS} is based on DFT total energies and included for reference. For ease of comparison, G°_{TS} and E°_{TS} in this table are relative to the free and total energies, respectively, of gas-phase ethanol plus a balance of gas-phase H_2.

Green Chemistry Accepted Manuscript

Table 8: Temperature (T) dependent standard free energy (G^o) for gas-phase species and surface intermediates, including transition states, on Ru(0001) used to parameterize the microkinetic model for acetic acid hydrogenation to ethanol.

species	G^o
acetic acid$_{(g)}$	$-0.00318T - 44.795$
ethanol$_{(g)}$	$-0.00314T - 44.455$
water$_{(g)}$	$-0.00203T - 13.540$
$H_{2(g)}$	$-0.00144T - 6.370$
acetyl*	$-0.00109T - 35.004$
acetaldehyde*	$-0.00103T - 38.084$
ethoxy*	$-0.00117T - 41.788$
OH*	$-0.000430T - 10.602$
acetate*	$(0.00451T + 140.729)(2.219\theta_{ATA*}^3 - 1.135\theta_{ATA*}^2 + 0.161\theta_{ATA*} - 0.308)$
O*	$(0.000126T + 4.425)(0.0281\theta_{O*}^2 + 0.395\theta_{O*} - 1.752)$
H*	$(0.000470T + 30.032)(0.00469\theta_{H*}^2 + 0.00148\theta_{H*} - 0.127)$
TS1	$-0.00126T - 44.855$
TS2	$-0.000997T - 37.942$
TS3	$-0.00113T - 41.156$
TS4=TS_{hydrog}	$-0.00154T - 44.358$
TS5	$-0.000327T - 9.938$
TS6	$-0.000547T - 13.257$
TS8	$-0.00144T - 45.123$
TS9	$-0.00107T - 41.607$
TS_{decomp}	$-0.000946T - 38.068$

All energies are in eV. G^o for each species is calculated at the conditions of the temperature experiments and fitted to a linear function in T. For acetate, O, and H, G^o is the coverage-dependent differential standard free energy and θ^o is equal to θ. For all other species θ^o is 1/9 ML. H_2 dissociation on Ru(0001) is calculated to be barrier-less even with 7/9 ML of pre-adsorbed atomic H, so the standard free energy of activation of Step 7 is assigned a small arbitrary value of 0.10 eV independent of temperature, which does not affect the outcome of the microkinetic model. Multiple reactants or products in a step are calculated in separate unit cells.

Green Chemistry Accepted Manuscript

Table 9: Results of the microkinetic models for acetic acid hydrogenation to ethanol calculated at the conditions of the temperature experiments: rate of acetic acid conversion ($-r_1$), coverage of adsorbed species (θ), and reversibility for each step (β).

T (°C)	110	160	185
Two-site model			
$-r_1$ (1/s)	0.28	2.39	19
Ethanol selectivity (%)	72	71	52
Coverage (ML)			
*	1.4×10^{-4}	1.8×10^{-4}	4.1×10^{-4}
H*	0.84	0.62	0.61
O*	0.11	0.09	0.10
acetate**	0.05	0.29	0.29
Reversibility			
β_1	0.04	0.22	0.39
β_2	1.00	1.00	1.00
β_3	0.77	0.81	0.83
β_4	0.01	0.09	0.15
β_5	0.48	0.61	0.68
β_6	0.02	0.05	0.08
β_7	1.00	1.00	1.00
β_8	1.00	1.00	1.00
β_9	1.1×10^{-5}	6.5×10^{-5}	2.3×10^{-4}
Partial pressure (bar)			
acetic acid	3.3×10^{-2}	0.21	0.45
ethanol	1.3×10^{-2}	0.38	0.86
H_2O	1.43	6.14	11.18
H_2	50.23	44.98	39.21
Reaction quotient	3.2×10^{-11}	3.2×10^{-8}	6.2×10^{-7}
One-site model			
$-r_1$ (1/s)	33	171	819
Ethanol selectivity (%)	85	80	63
Coverage (ML)			
*	6.6×10^{-5}	1.1×10^{-4}	2.6×10^{-4}
H*	0.75	0.53	0.52
O*	0.20	0.18	0.18
acetate*	0.05	0.29	0.29
Reversibility			
β_1	0.71	0.83	0.85
β_2	1.00	1.00	1.00
β_3	0.77	0.79	0.81
β_4	2.4×10^{-5}	5.9×10^{-4}	2.1×10^{-3}
β_5	0.76	0.87	0.88
β_6	3.7×10^{-5}	2.5×10^{-4}	8.9×10^{-4}
β_7	1.00	1.00	1.00
β_8	0.94	0.96	0.97
β_9	0.99	1.00	1.00
Partial pressure (bar)			
acetic acid	3.3×10^{-2}	0.21	0.45

Green Chemistry Accepted Manuscript

ethanol	1.5×10^{-2}	0.43	1.04
H_2O	1.43	6.14	11.18
H_2	50.23	44.93	39.03
Reaction quotient	3.5×10^{-10}	8.3×10^{-8}	1.1×10^{-6}
Equilibrium constant	34.29	6.87	3.51

Equilibrium constant is based on gas-phase acetic acid hydrogenation to ethanol. Reaction quotient is equal to $\prod_{i=1}^{9}\beta_i$.

Green Chemistry Accepted Manuscript

Figures

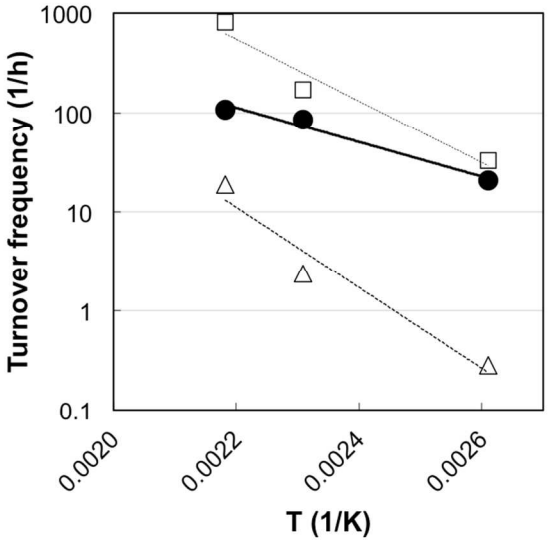

Figure 1: Carbon turnover frequencies of acetic acid hydrogenation on Ru/C at 750 psi total pressure and 110-185°C in the 3-phase flow reactor (●; the temperature experiments). See Table 1 for experimental parameters. The turnover frequencies of acetic acid conversion predicted by the microkinetic models at corresponding experimental conditions are plotted for comparison. △: two-site model; □: one-site model.

Green Chemistry Accepted Manuscript

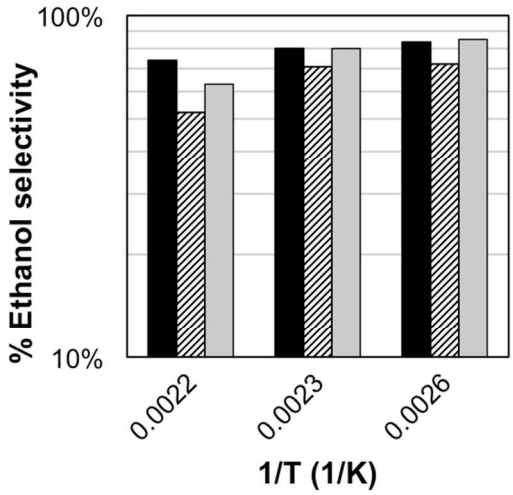

Figure 2: Ethanol selectivity in acetic acid hydrogenation on Ru/C at 750 psi and 110-185°C in the three-phase flow reactor (black bars). See Table 1 for experimental parameters. Striped and grey bars are ethanol selectivity predicted at corresponding experimental conditions, using the two-site and one-site models respectively.

Green Chemistry Accepted Manuscript

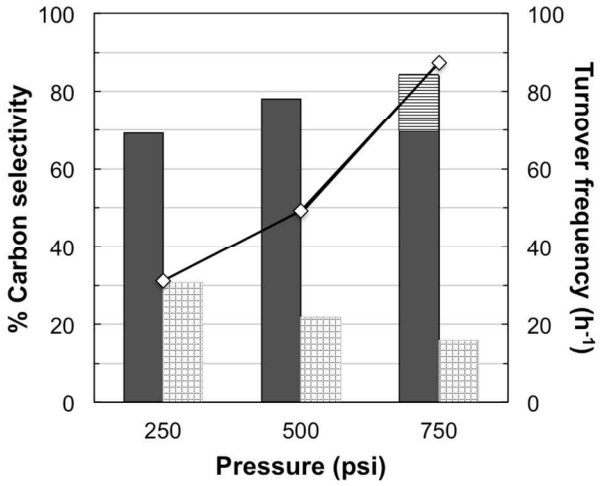

Figure 3: Ethanol selectivity and carbon turnover frequency for acetic acid hydrogenation at 160°C and three different pressures on Ru/C in the three-phase flow reactor. Black: ethanol+ethyl acetate selectivity; check: methane+ethane selectivity; points: turnover frequency. The percentage due to ethyl acetate in the liquid phase is indicated for 750 psi only (striped area). See Table 3 for experimental parameters.

Green Chemistry Accepted Manuscript

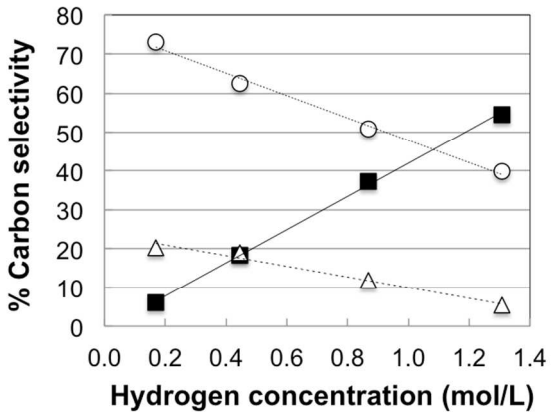

(a)

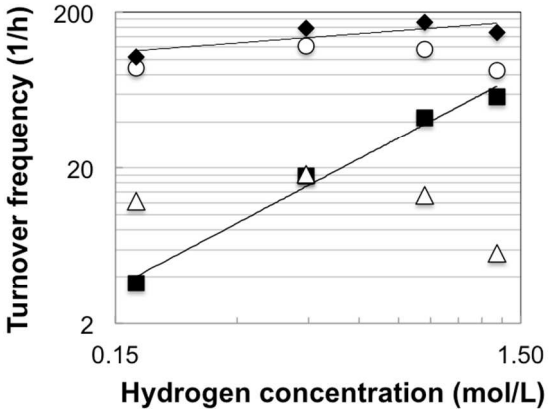

(b)

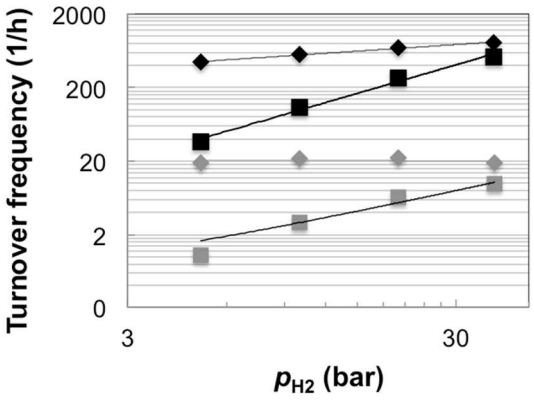

(c)

Figure 4: Effect of hydrogen concentration on the (a) selectivity and (b) turnover frequencies of acetic acid and the major products in acetic acid hydrogenation at 750 psi and 185°C on Ru/C in the three-phase flow reactor. No ethyl acetate is produced. See Table 4 for experimental parameters. (c) turnover frequencies of acetic acid conversion and ethanol formation predicted using the microkinetic models and selectivity descriptor. ◆: acetic acid; ■: ethanol; ○: methane; △: ethane. In (c), black symbols are results of the one-site model and the grey symbols are the results of the two-site model.

Green Chemistry Accepted Manuscript

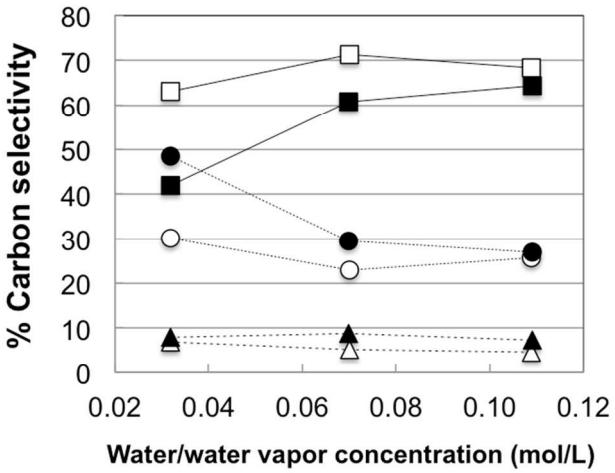

(a)

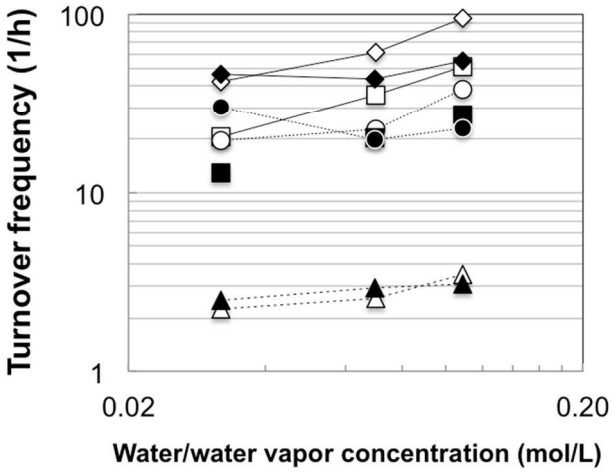

(b)

Figure 5: Effect of water concentration on (a) product selectivity and (b) turnover frequency in acetic acid hydrogenation at 185°C on Ru/C in the two- and three-phase flow reactors. ◆◇: acetic acid; ■□: ethanol; ●○: methane; ▲△: ethane; hollow symbols: two-phase; filled symbols: three-phase. See Table 5 for experimental parameters.

Green Chemistry Accepted Manuscript

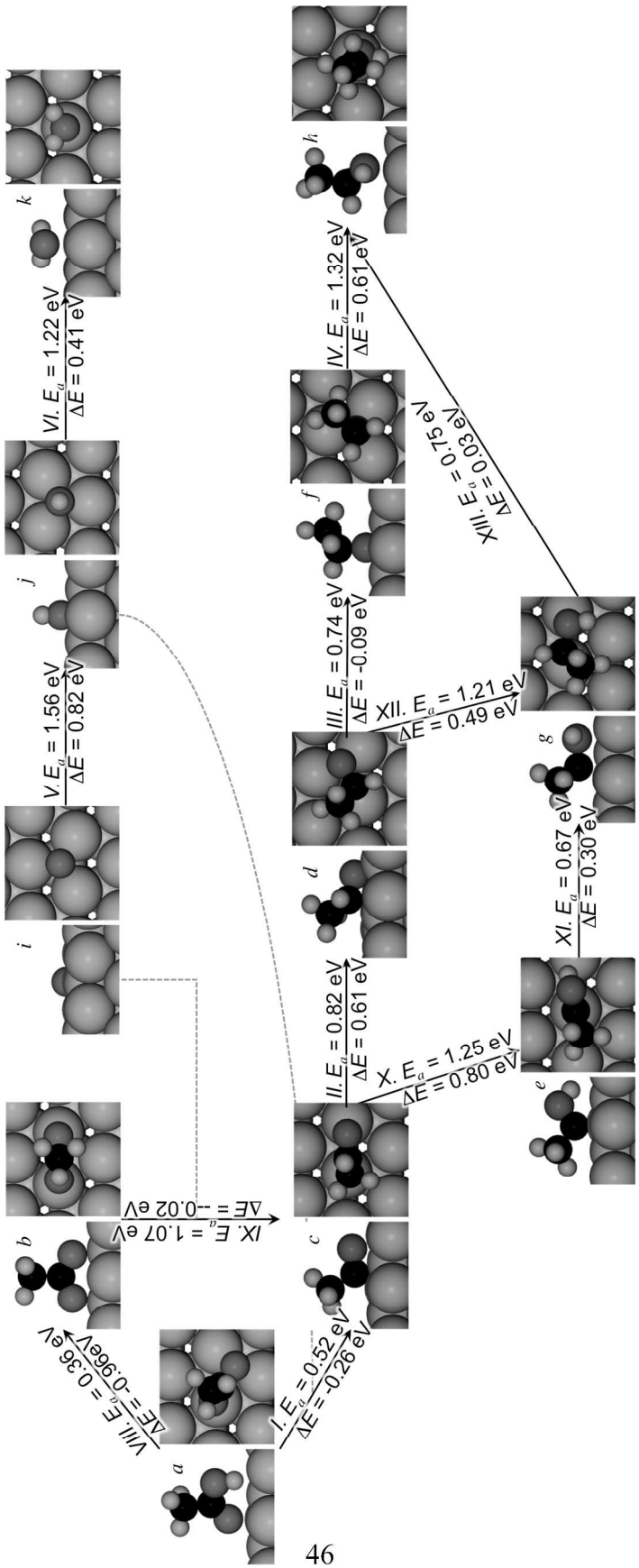

Green Chemistry Accepted Manuscript

Figure 6: Reaction network for the formation of ethanol from acetic acid hydrogenation. Only the selective pathways are shown. The surface intermediates on Ru(0001) are: (a) acetic acid; (b) acetate; (c) acetyl; (d) acetaldehyde; (e) 1-hydroxyethylidene; (f) ethoxy; (g) 1-hydroxyethyl; (h) ethanol; (i) O; (j) OH; (k) H_2O. Snapshots for the minimum-energy configuration for each intermediate are included (in each panel, left: side view; right: top view). Large grey, medium grey and black, and small white spheres represent Ru, O, C, and H atoms, respectively. The DFT-calculated total energy forward activation energy (E_a) and reaction energy (ΔE) for each elementary step are indicated on each arrow.

Green Chemistry Accepted Manuscript

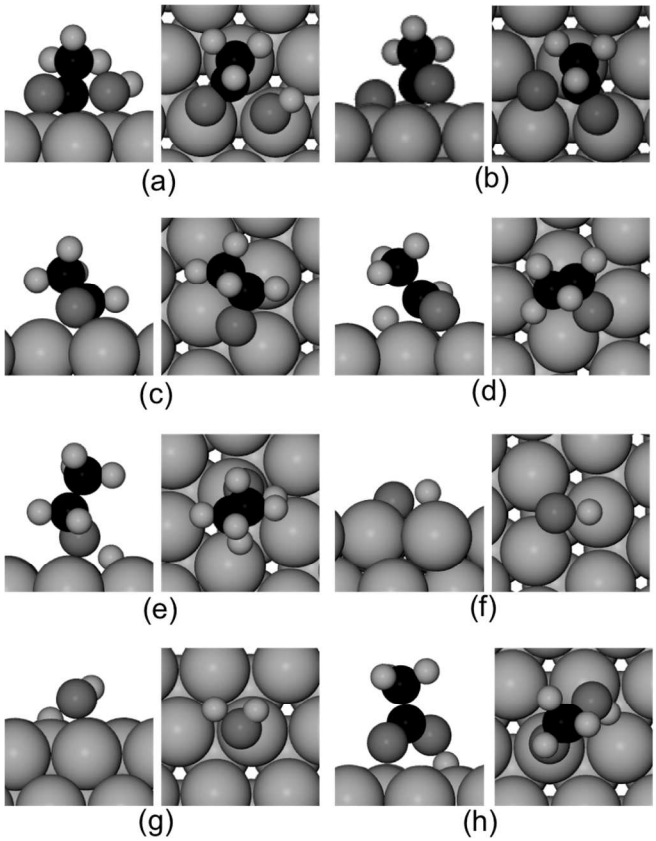

Figure 7: Snapshots of the transition states of the steps included in the microkinetic models: (a) acetic acid→acetyl+OH; (b) acetate→acetyl+O; (c) acetyl+H→acetaldehyde; (d) acetaldehyde+H→ethoxy; (e) ethoxy+H→ethanol; (f) O+H→OH; (vii) OH+H→H_2O; (g) acetic acid→acetate+H. In each panel, side view is on left and top view is on right. Large grey, medium grey and black, and small white spheres represent Ru, O, C, and H atoms, respectively.

Green Chemistry Accepted Manuscript